
Proceedings Paper:
Dewulf, L., Hausmann, M.K., Bozon, A. et al. (3 more authors) (2024) Food vs packaging: dynamics of oil migration from particle systems into fibrous material. In: Palzer, S. and Niederreiter, G., (eds.) Powder Technology. 10th International Granulation Workshop, 21-23 Jun 2023, Sheffield, United Kingdom. Elsevier BV. Article no: 119721. ISSN: 0032-5910. EISSN: 1873-328X.

https://doi.org/10.1016/j.powtec.2024.119721

Powder Technology 439 (2024) 119721

Contents lists available at ScienceDirect

Powder Technology

journal homepage: www.journals.elsevier.com/powder-technology

Food vs packaging: Dynamics of oil migration from particle systems into fibrous material

Luc Dewulf [a,*], Michael K. Hausmann [b], Annabel Bozon [c], Gerhard Niederreiter [b], Stefan Palzer [b], Agba D. Salman [a]

[a] Department of Chemical and Biological Engineering, University of Sheffield, Mappin Street, Sheffield S1 3JD, United Kingdom
[b] Nestlé Research, 1000 Lausanne, Switzerland
[c] Nestlé Product Technology Centre, Lange Straße 21, 78221 Singen, Germany

HIGHLIGHTS

- Particle size reduction from 500 to 50 μm made stronger capillarity in particle system.
- Undesired oil-release into paper packaging was essentially stopped to 0%.
- Raman chemical imaging (RCI) was successfully used first-time for oil quantification.
- Optical oil stain quantification on paper was automated for fast result acquisition.
- Larger particle system leaked 50% of oil into packaging, smaller particle system 0%.

GRAPHICAL ABSTRACT

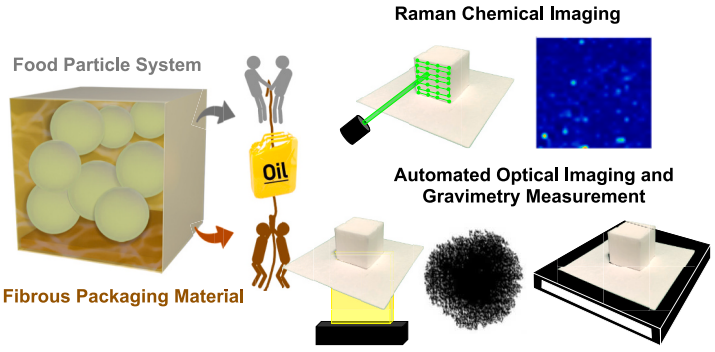

ARTICLE INFO

Keywords:
Particle and fibre packaging systems
Quantitative Raman laser chemical imaging
Oil migration
Oil release
De-oiling

ABSTRACT

Paper packaging for compacted or tabletted foods is seen as a key sustainable packaging of the future. Yet its fibrous structure is susceptible to absorb oils, fats, greases and other small molecules from the contacting food. Underlying phenomena associated with oil release from compacted food on fibre-based packaging, such as viscous liquid flow, capillarity, and gravity from compacted particle systems into fibre networks are not fully understood yet. As such, oil stain mitigation on packaging remains a challenge. Using model food tablets of 95% 500 and 50 μm particle size with 5% sunflower oil as the liquid phase, this work employed for the first-time quantitative Raman spectroscopic chemical imaging (RCI) coupled with automated image quantification for comparison of oil flow dynamics between food compacts and contacting paper packaging. The extent of de-oiling from the compact and imbibed into paper showed similar exponential decay with time for both porous systems. For the first time, oil migration dynamics on the food compact surface was 2D visualised via Raman spectroscopy and showed markedly different trends with varying environment climatic conditions and compact microstructure. The larger particle system leaked up to 50% of oil into paper, whereas the 50 μm system retained 100% of its oil, creating an effective internal oil barrier. This novel technique opens the way for further understanding liquid transfer between porous food media and harnessing microstructure engineering to increase food and packaging performance.

* Corresponding author.
E-mail address: ldewulf1@sheffield.ac.uk (L. Dewulf).

https://doi.org/10.1016/j.powtec.2024.119721
Received 29 November 2023; Received in revised form 24 March 2024; Accepted 28 March 2024
Available online 29 March 2024

1. Introduction

Pressured by changing consumer behaviour, fast moving packaged goods companies around the world pledge to become more environmentally sustainable by reducing conventional packaging, especially plastic and metal [1]. Due to its comparatively high tensile strength, paper is currently used to reinforce multilayer sandwich packaging, with plastic or metal layers to provide necessary barriers against small molecules migration. However, the absence of moisture or oxygen barrier properties of paper limit its use in the food sector to products that are less susceptible to environmental conditions. Paper packaging enjoys high consumer acceptance due to its biodegradability, potential carbon neutral sourcing, and psychological effects related to haptics and optics [2]. Yet, a significant disadvantage of paper or indeed of any other fibrous food-contact material is its propensity to absorb mobile substances from the food, such as oils, fats, and greases [3]. With increasing employment of paper as a food-contact wrapping material, attempts to understand, model, and control oil and fat migration from food to packaging is timely and relevant.

Food systems in powder, granular, tableted, or compacted form and fibrous packaging materials resemble each other in the sense that both are porous media in contact with each other, and thus fundamental phenomena apply to both systems. A food system (such as a seasoning compact) comprising particulate ingredients and a liquid component (such as oil) in contact with a fibrous packaging material (such as paper) undergoes a transport phenomenon whereby the mobile substance transfers from the food into the paper, which is often referred to as oil release [4], oil migration [5], or de-oiling, where the three are used synonymously. Regarding oil release, the commonality is thus that the particle-based food system and fibre network packaging are both stationary porous media with oil migrating from one porous phase to the adjacent.

Literature makes proof of considerable work having been conducted on liquid transport into porous material. Washburn pioneered the explanation of liquid transport into porous beds via capillary suction formulating the Washburn Eq. [6]. The work was then extended from powder systems to other porous structures, such as fibrous media like fabric or paper, which have been well reviewed [7–9]. Relating to packaged consumer foods, the process of oil imbibition into paper via wetting and capillary suction is therefore fundamentally rather well understood.

On the other hand, considerably less work has been conducted on liquid flow out of porous media or between porous phases. Literature shows that the flow of liquid out of particle systems shows time-dependent behaviour, affected by liquid saturation, capillarity, and gravity, as was demonstrated for the case of glass spheres in a packed bed [10]. In their study, the amount of liquid holdup within the bed was measured during natural gravity drainage. The amount of liquid retained was larger in a capillary dominated regime, and thus the liquid outflow was larger in a gravity-dominated regime.

From the literature on liquid flow processes in porous and fibrous bodies it can be summarised that the extent of liquid phase transfer between bodies depends on gravity, viscous flow, and capillarity effects in both particle and fibre system, schematically summarised in Fig. 1. During imbibition, diffusion is rather considered a slow process occurring after capillary suction [11] and therefore unlikely to play a role in immediate oil imbibition into paper, although in long-term food shelf-life tests disagreement still exists over which processes dominate [5].

Real food compacts are wrapped in packaging from all sides with potential contact between food and paper on all faces. For experimentation however, simplification into a 1D system is appropriate and confines the oil flow direction to the vertical, either up or down akin to a tug competition for oil between food and paper. Attraction due to the earth's gravitational acceleration always acts as a downwards force, in the current setup favouring imbibition into paper. Pressure drop due to viscous laminar flow is theoretically present in both porous materials, but is more pronounced in food as the smaller pore size in paper can overcome the viscous pressure loss. For a basic pipe flow geometry, this can be modelled with the Hagen-Poiseuille Eq. [12]. In the competition for oil, a larger viscous flow resistance would result in a prolonged retention of oil in the food structure. While viscous effects act as a resistance to oil flow, capillarity is the driving force in porous media, stemming from the pressure drop across the meniscus in the solid-liquid-gas region, calculated for a simple capillary geometry from the Laplace-Young Eq. [13]. Depending on the relative magnitude of the resulting capillary forces, the oil will be drawn into the paper or possibly retained in the food.

In order to better understand this dynamic behaviour of liquid outflow from porous material, it becomes clear that sophisticated experimental methods are required. Recently, advanced imaging, non-invasive and non-destructive techniques for particle system microstructure have been developed [14]. Microscopic techniques have rapid acquisition times, but capture processes on the sample surface, while tomographic methods reach the internal structure but suffer from acquisition times possibly much longer than the timescales of the transport processes within the sample. A potentially powerful analysis method yet underutilised for liquid-particle systems is Raman laser spectroscopy. Raman spectroscopy is a spectroscopic technique in which a monochromatic light, e.g., from a laser, is shone on a sample and the inelastic backscattering (stokes scattering) is quantified by measuring the number of photons excited or absorbed, expressed as intensity. For a sample to exhibit a Raman effect, the molecule must be polarisable, which is overwhelmingly the case in covalently bonded samples such as in most organics, but not in purely ionic species without shared electrons. As such, Raman spectroscopy is suitable to monitor temporal and spatial behaviour of an organic phase migrating through an inorganic phase.

Raman-based techniques have been used widely across the food science domain for analytical purposes of food safety and authenticity control [15–17]. In these cases, measurements at a single point in location and time of the bulk material is often sufficient. Much less reported in the food sector is quantitative Raman chemical or hyperspectral imaging (RCI) or mapping. Few previous examples exist, such as RCI to map the distribution of nutrients in fruit and vegetables [18] and of different tissues in meat [19] and other frozen foods [20]. For food powder systems, mixing efficiency of corn-flour and icing sugar was evaluated via RCI [21]. Application of RCI techniques in tablets and compacts has only been reported for pharmaceutical tables, not yet in the food domain. In pharma, main objectives were spatial mapping of active pharmaceutical ingredient distribution [22,23], disintegrant

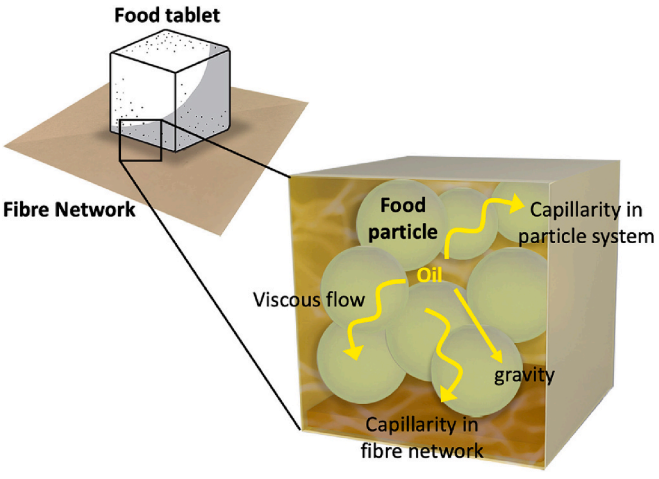

Fig. 1. Schematic of different drive (fibre capillarity, gravity) and resistance (food capillarity, viscosity) processes occurring during oil release from particle food systems to fibre-based packaging.

[24,25], and impurities [26], or the differentiation between polymorphs [27,28]. The common difficulty in Raman scanning of irregular surfaces was addressed in a study on convex tablets [29], and coverage of tablet coating [30]. Yet, as in previous studies, all systems were solid-phase and static, whereby RCI of dynamic liquid-solid systems have been unreported in food and pharma. For such systems, few examples exist such as in two-component liquid mixing in aerospace flows [31], or the coupling of RCI with seed particles for particle image velocimetry [32–34]. However, the application of RCI for profiling fluid transport in particle-based compacted food systems remains unreported.

Similar to particle-bed systems, imbibition of liquid into fibrous material such as paper has been shown to be a dynamic time-dependent system. While due to the small interstitial pore size between fibres the flow regimes are more influenced by capillarity than gravity, the finite medium thickness (i.e. paper thickness) and sheet size, as well as fibre swelling results in an unsteady system (i.e. non-constant with time) [35]. Previous work aiming to establish the dynamics of oil imbibition into paper, on a fundamental level [36,37] or specifically for food packaging [38], used photographic oil stain measurements, that are still often evaluated manually. In addition, oleogels were used and as such reports of the interaction between particulate systems in contact with fibrous material remain little reported.

Conclusively, while work on the individual processes and the resulting dynamic behaviour for liquid transport into porous bodies has been reported previously, the complexity of mass transfer between two porous bodies, specifically between particulate food systems and fibrous packaging is less well described in literature. This work will contribute towards a better understanding of the dynamic behaviour of liquid migration between particulate food powder systems and fibrous packaging, ultimately aiming to control this unwanted phenomenon in the consumer foods industry. Raman laser spectroscopy is applied for the first time to evaluate dynamic liquid flow distribution in particle systems, and self-written automated imaging software is used for evaluation oil flow dynamics in fibre networks.

2. Materials and methods

To model a typical food system prone to de-oiling, a model food compact was created using 95 w/w% table salt and 5 w/w% sunflower oil manually mixed in 100 g portions a beaker by adding first the salt and then oil. Table salt was obtained from Südwestdeutsche Salzwerke AG and sieved to a fraction of 500–600 μm for sample A and B, and 50–60 μm for sample C using sieves (AS 200 Basic, Retsch, Haan, Germany). High oleic sunflower oil was obtained from Olam, Singapore, and viscosity measured rheometrically as 73 mPa.s at 20 °C and 59 mPa.s at 30 °C at a shear rate of 0.1 s^{-1} in the bob and cup geometry (Kinexus Pro, Malvern, UK).

After mixing, for each food compact 4 g of salt+oil mixture were compacted in a 14 × 14 mm square die to a height of 13.5 mm using a universal testing machine (3367, Instron, Norwood, MA), resulting in a compact density of 1.5 g/cm^3. Salt+oil compacts were subjected to oil release measurements within 30 min of compacting by placing on a paper substrate at 20 °C (sample A) and 30 °C (sample B and C) environment temperature. To model fibrous packaging material, blotting paper (3MM CHR, Whatman, Marlborough, MA) was used, with true density 1.55 g/cm^3, and cut to squares of 8 × 8 cm. The procedure is summarised in Fig. 2.

2.1. Quantitative Raman chemical imaging

Raman measurements of the compact surface were carried out once per day over 4 days by scanning a grid of 14 × 13.5 mm at 0.5 mm increments, resulting in 812 individual spectra. The compact was moved to each position by an xyz micrometer stage (SM 3.25, Märzhäuser, Wetzlar, Germany). To avoid focus errors, the compact was kept in the experimental setup over the 4 days, resulting in a single compact subjected to Raman imaging per sample A, B, and C. The laser source was a green 532 nm diode continuous wave laser (LCX, Oxxius S.A., Lannion, France) at the minimum possible setting of 94 mW power to avoid heating the sample. The beam diameter was measured as approximately 700 μm by measurement with the integrated photographic camera. The surface temperature of the compact when exposed to laser light was measured as 30 °C with a handheld infrared laser. Raman signal was acquired with a spectrometer (iHR320) with 1800 groves/mm, 500 nm blaze grating, and CCD camera (Synapse Plus, Horiba, Longjumeau, France). Signal acquisition time was 5 s and accumulated over 3 repeated measurements. The integral peak intensity was then calculated at each time and location point in order to trace the oil flow dynamics according to

$$I = \int_{\omega_0}^{\omega_n} i_\omega = \sum_{\omega_0}^{\omega_n} i_\omega \tag{1}$$

where I is the integral intensity (a.u.), ω_0 and ω_n are the lower and upper

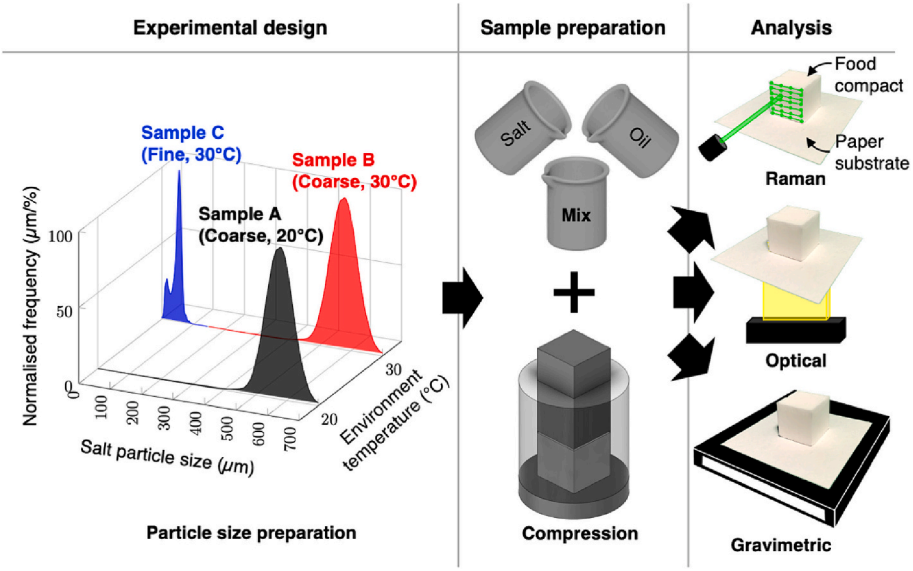

Fig. 2. Summary of experimental design, sample preparation and analysis of oil release from food compacts into paper.

spectral limits respectively (cm^{-1}), and i_ω is the intensity (a.u.) at each Raman shift ω. The measured peak intensity was then converted to oil concentration based on a calibration curve constructed by performing Raman imaging on three compacts each of a set of 15 compacts with 0, 2.5, 5, 7.5, and 10 *w*/w% oil and the balance salt. Oil concentration was then mapped on the initial measurement grid to construct 2D images of the local surface oil distribution of the compact with a resolution of 812 pixels on a 0.5 × 0.5 mm raster. In addition, the surface oil concentration averaged over the entire sample image was evaluated by

$$\bar{c} = \frac{\int_{p_0}^{p_n} p_p c_p}{\int_{p_0}^{p_n} p_p} = \frac{\sum_{p_0}^{p_n} p_p c_p}{\sum_{p_0}^{p_n} p_p} \tag{2}$$

where $\bar{c}$ is the average surface oil concentration (w/w%), p_0 and $p_n$are the first and last pixel in the image respectively, and c_p is the oil concentration (w/w%) evaluated at each pixel p_p.

2.2. Optical oil stain quantification

Optical measurements of the oil stain on paper were carried out every 12 h over 4 days from the underside of the paper in triplicate measurements. The compacts were removed only during the rapid optical scanning and then placed back on exactly the same positions on the paper substrate with the help of reference points printed on the top side of the sample paper. Due to refractive index matching of oil and paper fibres, light transmission of oil-imbibed paper is greatly enhanced in contrast to oil-free paper with more scattering, and thus resulting in different grey values [36]. By calibrating the ratio of pixel to actual distance on paper, the number of darker pixels was converted to oil stain area in cm^2, filtered for noise in samples with obvious oil stains, and unfiltered for sample with no obvious oil stains.

2.3. Gravimetric measurement

Gravimetric measurements of oil imbibed into paper were similarly carried out every 12 h over 4 days in triplicates on an analytical balance (Precisa 125 A, Mettler Toledo, Nänikon, Switzerland). For each measurement, the food compact was removed from the paper substrate and the paper weighted, tared to its initial weight without oil at the beginning of the experiment.

3. Results and discussion

3.1. Raman calibration

In a first step, Raman spectra of pure salt and sunflower oil were acquired over the range 0 to 3500 cm^{-1} and the peaks annotated with values generally accepted in literature (Fig. 3). As high oleic sunflower oil is a mixture of mostly oleic- and linoleic acid-derived triacylglycerides, there is no unique spectrum but instead different peaks associated with molecular vibrations occurring in the functional groups of the different oil components (Table 1) [39,40]. As expected, the spectrum of pure salt is free of peaks and close to the baseline, allowing a clear discrimination between salt and oil. Moreover, the experimental peaks are congruent with reported literature peak values, giving confidence in the acquisition method [39,40]. To avoid lengthy measurements over the entire spectrum, spectra were only collected between 2800 and 3050 cm^{-1}, as this region has three prominent peaks of the sunflower oil fingerprint, as shown in the inset of Fig. 3.

For the quantification of the surface oil concentration on the compact in terms of concentration and not solely Raman intensity, a calibration curve was constructed for each salt+oil compacts made from coarse salt

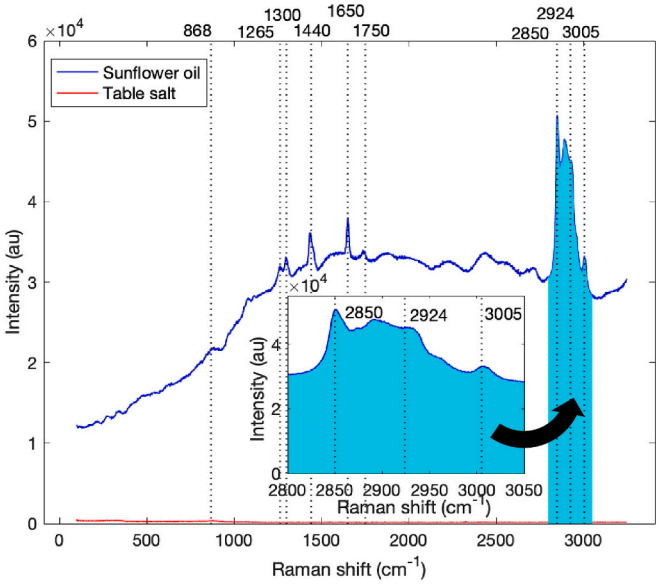

Fig. 3. Acquired full range Raman spectrum of pure salt (blue line) and sunflower oil (red line) with annotated literature peaks [39,40]. Inset shows the selected range from 2800 to 3050 cm^{-1} chosen for further quantitative Raman chemical imaging. (For interpretation of the references to colour in this figure legend, the reader is referred to the web version of this article.)

Table 1
Generally accepted major Raman peaks in edible oils, adapted from [39,40].

Raman shift (cm^{-1})	Vibration mode	Functional group
868	C–C stretching	$-(CH_2)_n-$
968	C = C bending	trans RHC=CHR
1008	CH_3 bending	$HC-CH_3$
1150	C–C stretching	$-(CH_2)_n-$
1265	=C–H bending (scissoring)	cis RHC=CHR
1300	C–H bending (twisting)	$-CH_2$
1440	C–H bending (scissoring)	$-CH_2$
1525	C=C stretching	RHC=CHR
1650	C=C stretching	cis RHC=CHR
1750	C=O stretching	RC=OOR
2850	C–H symmetric stretching	$-CH_2$
2897	C–H symmetric stretching	$-CH_3$
2924	C–H asymmetric stretching	$-CH_2$
3005	=C–H symmetric stretching	cis RHC=CHR

for samples A and B, and salt+oil compacts made from fine salt for sample C. Fig. 4 shows the calibration spectra of the coarse samples. As expected, the 0 w/w% oil sample is parallel to the baseline, while increasing oil concentrations in the calibration compacts resulted in increasing spectral intensities, with almost equal distance between spectra for each 2.5 w/w% oil concentration increase. Fig. 5 shows the resulting calibration curve of integral intensity calculated with Eq. (1) against compact oil concentration. While the large error bars result from the large variations in spectra for each sample, it is still possible to evaluate a linear trend by least squares regression given as $I = 2.142 \times 10^5\, c + 4.255 \times 10^5$ with $R^2 = 0.97$.

Fig. 6 similarly shows the calibration spectra for compacts from fine salt particles. The intensities are generally about 5 times as large and converge for the 7.5 and 10 w/w% samples. This could be due to the fact that dispersing oil homogenously in fine powder is less efficient compared to coarse powder, some clumps and agglomerates were observed in the fine compacts. Fig. 7 shows the calibration curve for the fine samples given as $I = 2.2446 \times 10^6\, c + 2.513 \times 10^6$, with $R^2 = 0.87$ reflecting the larger variations in the fine sample calibration.

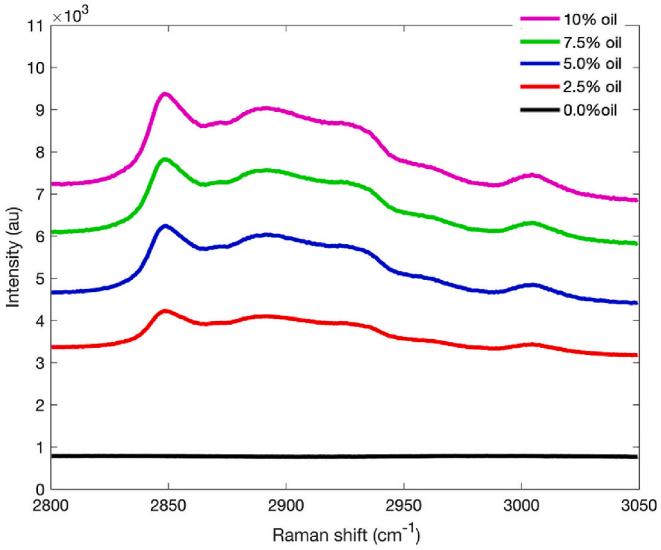

Fig. 4. Acquired Raman calibration spectra for salt+oil compacts made from coarse salt.

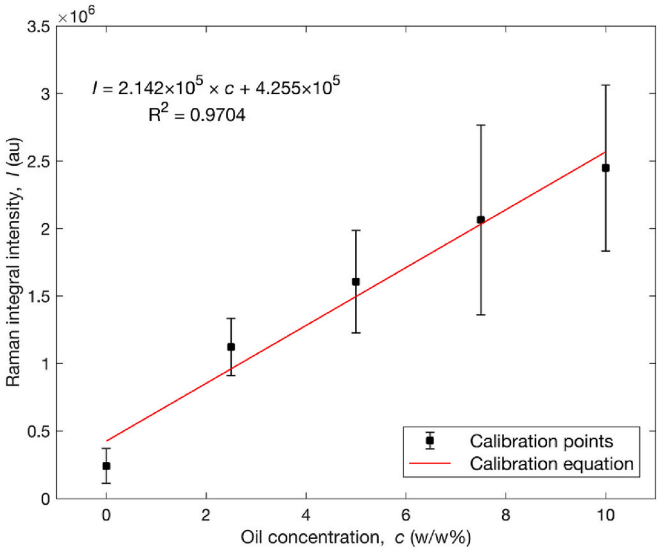

Fig. 5. Calibration curve for salt+oil compacts made from coarse salt.

3.2. Quantitative Raman chemical imaging

After calibration, salt+oil compacts were prepared according to the procedure in Fig. 2 and placed on paper substrate for analysis. The Raman spectra of the compact surface, converted to surface oil concentration and reconstructed in 2D quantitative Raman chemical images are shown in Fig. 8, where the x and y axes represent width and height of the compacts respectively, and the z axis is represented as a colour scale from 0 to 100 w/w% oil concentration. Generally, all three samples exhibit an overwhelmingly blue colour, indicating a concentration around 0 to 10 w/w% oil, as expected due to the 95 w/w% salt and 5 w/w% initial oil concentration. Sample A and B contain distinct spots of high oil concentration up to 100 w/w% oil (red colour), which could be attributed to the larger particle size and thus larger liquid bridges formed, which contain a high oil concentration, in addition to variability induced by manual mixing. The fact that the high concentration clusters are in the same locations over the 4 days confirms that they are not artifacts. Conversely, the surface colour of sample C appears more homogenous, likely due to the smaller particle size and smaller oil bridges.

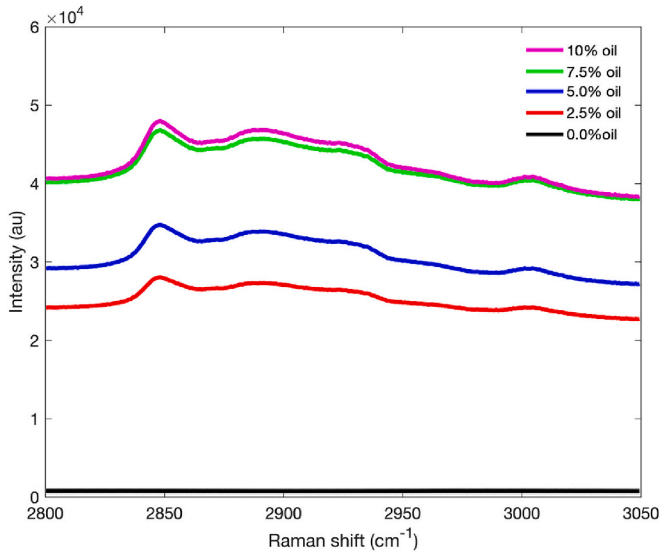

Fig. 6. Acquired Raman calibration spectra for salt+oil compacts made from fine salt.

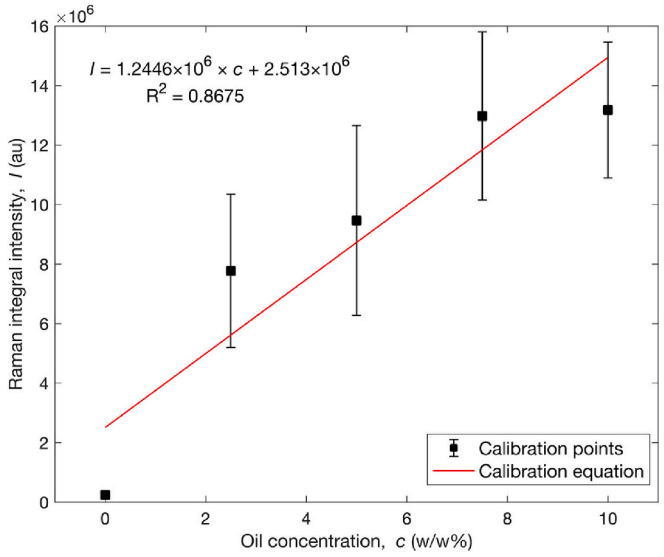

Fig. 7. Calibration curve for salt+oil compacts made from fine salt.

While some areas show 1–2 mm diameter agglomerates with higher oil concentration, the overall concentration is more evenly distributed than in the coarse samples with individual pixel-sized hotspots. The increasing homogenous distribution of liquid between coarse and fine particle systems was previously described for liquid imbibition into tablets and powder beds [41,42], but is likely also applicable to the reverse process of liquid release in this study. Comparing the samples over time, changes in particle size (sample B vs C) have a much more drastic effect than temperature at a fixed particle size (sample A vs B). This is manifested by the fact that the oil concentration changes little in the 4 days of sample C, suggesting more oil is retained. On the other hand, sample B shows stark changes from areas of up to 40 w/w% down to 0. Colour comparison between sample A and B shows that for the same particle size but different temperature, the concentration drop is only marginally slower in sample A compared with sample B.

In addition to the novel Raman chemical imaging for picturing previously unknown surface oil dynamics, average and normalised average ($t_0 = 100$ w/w%) surface oil concentration against time, calculated from Eq. (2), was plotted in Fig. 9. Comparison of the three samples shows

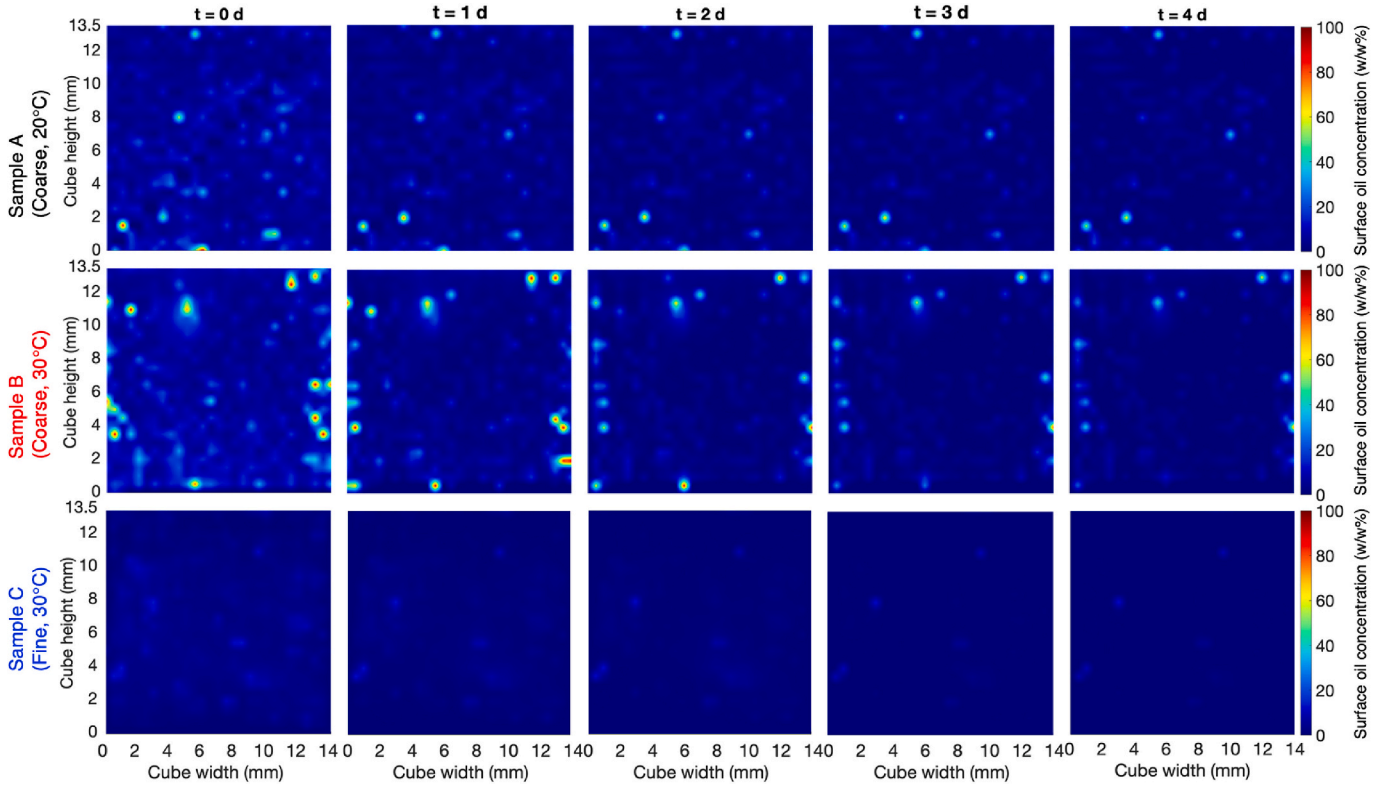

Fig. 8. Quantitative Raman chemical images of sample A, B, and C showing the dynamic behaviour of surface oil concentration on the faces of salt+oil compacts in contact with paper substrate.

that all three food compacts have reducing surface oil concentrations, with samples A and B having the most drastic change from 6.5 and 9.5 w/w% initially to 2 w/w% after 4 days for both samples. As expected, sample B has a minimally faster oil release of in total (9.5–2)x100/9.5 = 80%, compared to 70% for sample A, owing to the higher temperature and resulting lower oil viscosity of 59 mPa.s for sample B compared to 73 mPa.s for A. Sample C loses oil slowest from 3 to 0 w/w%. Although the nominal initial oil concentration was 5 *w*/w% in all samples, the variations in initial concentrations could be due to the time lag between compaction and sample measurement, due to the Raman analysis duration of 5 h until all 812 data points were sampled, or due to the phenomenon that liquid is forced to the sides of a tablet during compaction, which has previously only been reported for extrusion [43]. The latter argument is supported by hotspots in Fig. 8 being mostly located at the edges of compact samples A and B. The large spread in data for samples A and B indicated by the large error bars reflects the local variation from 0 to 100 w/w% in both samples in Fig. 8, whereas sample C has less concentration variation in Fig. 8 (0–30 w/w%) and thus less data spread in Fig. 9. Given the measured laser beam diameter of approximately 700 μm, the probing beam is similar in size to the particles in the coarse compact, and hence in extreme cases either an oil pocket or salt crystal was probed, resulting in stark differences in surface oil concentrations. In the fine compact, the ratio of laser beam diameter to particle size is larger and the additional smaller oil bridges mean more averaged local salt+oil mixtures are probed, and the event of sampling pure oil pockets or pure salt particles occurs seldom.

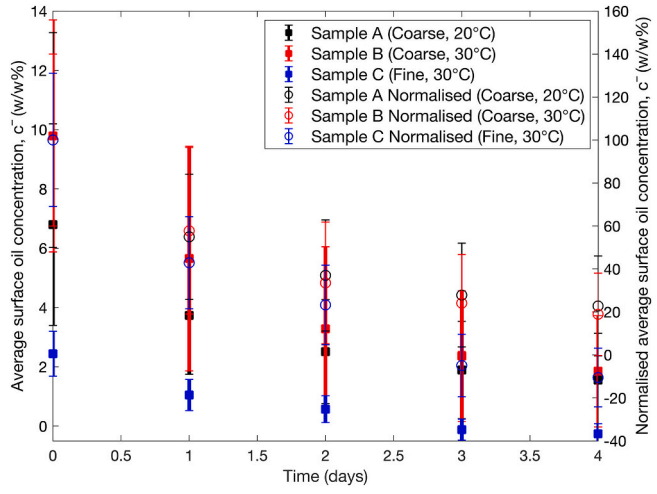

Fig. 9. Average and normalised average (t_0 = 100 w/w%) surface oil concentration obtained from Raman chemical images using Eq. (2) for each sample over 4 days.

3.3. Optical quantification

Techniques to measure oil transport in paper and other fibrous materials are much more established [36,37] and were used to validate the Raman chemical imaging measurements. Optical images of the underside of paper in contact with food compacts were taken and quantified via automated image analysis (Fig. 10). The increasing oil stain on paper for the coarse salt and oil compact (sample A, B) in contrast to the clear paper for the fine compact (sample C) confirm the trend seen previously in Raman chemical imaging. Similarly, the comparison of the same particle size at different temperatures seen in Raman chemical imaging is reflected by the larger oil stain at 30 °C compared to 20 °C. Fig. 11 shows the variation of quantified oil stain area over time in graphical representation, depicting the same trend seen previously. The same tendency of oil stain increase at early contact times and plateauing at later times has been previously seen for in the domain of echanical Engineering with lubrication grease blobs on blotting paper [36,37].

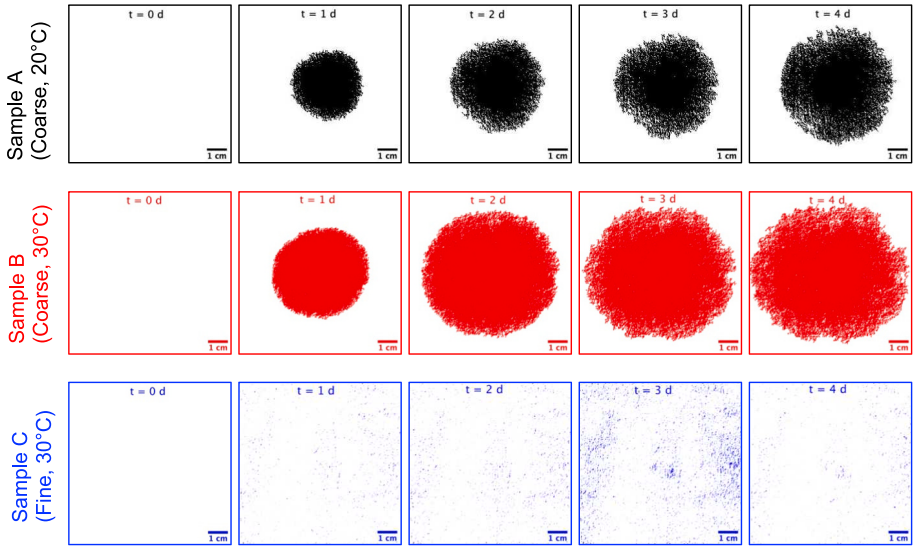

Fig. 10. Images of expanding oil stain measured via optical imaging and automated image quantification. The noise was filtered out for samples A and B with obvious oil stains but was not applied to sample C without obvious oil stains.

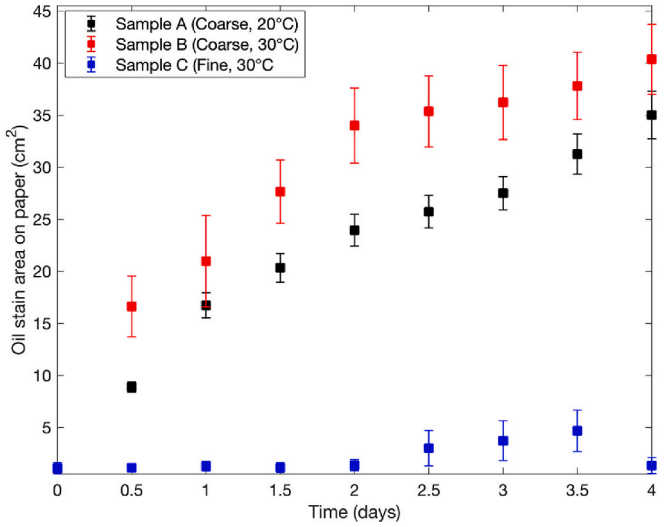

Fig. 11. Area of expanding oil stain over time measured via optical imaging and automated image quantification.

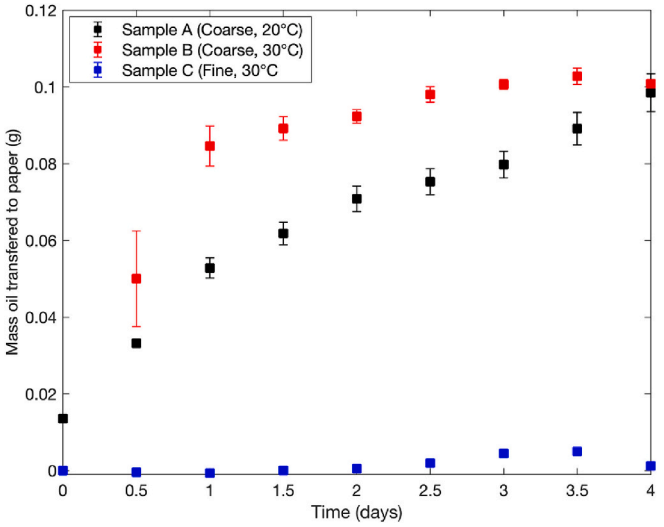

Fig. 12. Mass of oil transferred to paper over time measured gravimetrically.

3.4. Gravimetric analysis

Fig. 12 shows the mass of oil transferred from the food compacts into paper measured as the mass gain of the paper sample. Assuming a fixed paper grammage with isotropic porosity and constant thickness, the mass gain should follow the trend of automated oil stain imaging, in accordance with previous reports [36,37]. Indeed, sample A and B show increasing mass gain with time, showing a faster oil release at 30 °C compared to 20 °C and reaching similar final values of 0.1 g after 4 days, both observations being in accordance with the Raman chemical images in Fig. 8. and optical imaging in Fig. 10. Mass gain for Sample C is negligible following the trend of only minor changes from the spectroscopic and optical imaging. Given that each compact contained 5 w/w% = 0.2 g oil, the liquid hold-up of the coarse samples is only about half of the initial oil quantity (0.1 g), compared to almost the full 0.2 g oil for the fine samples.

The observed trend of increasing oil release at higher temperatures can be explained with the decreasing oil viscosity and thus easier flowability of oil from the food into paper at elevated temperatures. The observed trend of reduced oil release in food compacts of fine particles compared to large ones can be explained by the smaller inter-particle spacing in fine compacts, resulting in smaller radii of curvature and thus larger capillary forces according to the fundamental Young-Laplace Eq. [13]. The larger suction forces in small particle systems results in a higher retention of liquid in the system, which was confirmed in multiple works in the Chemical Engineering domain on water flow through separation columns packed with glass beads. For instance, liquid retention in a monodisperse 3 mm glass sphere bed was 3.1 w/w% of the initial fully saturated water content before drainage [10]. In another work employing 500 μm glass spheres, matching the particle size of sample A and B in this work, water retention was 5 w/w% [44]. The discrepancy to the 10 w/w% retention in the present work is therefore not only due to the reduced particle size, but also other parameters such as contact angle and viscosity. Another packed bed work employing an aqueous xanthan solution of 100 mPa.s viscosity, similar to the 75 mPa.s of sunflower oil used herein, achieved a maximum 4 w/w% liquid retention, albeit for 10 cm glass spheres [45]. Besides the thermodynamic effect of particle-size induced capillarity, the dynamic effect of increased fluid-wall friction plays a role [46]. As shown by reduced

dynamism in the Raman images for smaller particle sizes, the narrower inter-particle channel reduces the available hydraulic diameter and thus increases the viscous pressure drop according to the fundamental Hagen-Poiseuille equation, thereby slowing the flow [12]. In packed bed process flow applications, this phenomenon has been previously described with the Carman-Kozeny equation [47,48].

4. Conclusion

For the first time, it was achieved to concurrently measure oil release from a food compact into a fibrous packaging substrate by imaging the oil dynamics in both the food sample via quantitative Raman chemical imaging, and the paper substrate via gravimetry and optical imaging and automated quantification. Oil release from the food compact into paper was slightly reduced when the temperature was decreased from 30 to 20 °C, attributing this effect to the reduced oil viscosity. Oil release was almost completely stopped when the particle size was reduced from 500 to 600 to 50–60 μm, attributing this effect to the larger capillary suction and narrower channel diameter in the finer compact. The advantage of Raman spectroscopy was the ability of monitoring the oil release process locally and continuously or 'on-line', while paper-based techniques were discontinuous and only showed overall results. The analytical techniques developed in this work have been demonstrated by the findings to be highly useful in quantifying oil release from food into packaging. The results further show that an edible internal oil barrier can be created by reducing the particle size of the solid food fraction. This enables consumer food research to understand and develop more sustainable paper-based packaging compatible with oil containing foods. The next step of this research is suggested to be predictive modelling of the oil flow based on the physical properties of the porous and liquid systems.

CRediT authorship contribution statement

Luc Dewulf: Writing – review & editing, Writing – original draft, Visualization, Validation, Supervision, Software, Resources, Project administration, Methodology, Investigation, Funding acquisition, Formal analysis, Data curation, Conceptualization. **Michael K. Hausmann:** Supervision, Resources, Project administration. **Annabel Bozon:** Supervision, Resources, Project administration. **Gerhard Niederreiter:** Supervision, Funding acquisition. **Stefan Palzer:** Funding acquisition. **Agba D. Salman:** Writing – review & editing, Supervision, Funding acquisition.

Declaration of competing interest

The authors declare the following financial interests/personal relationships which may be considered as potential competing interests:

Luc Dewulf reports financial support was provided by Engineering and Physical Sciences Research Council. Luc Dewulf reports financial support was provided by Nestle Research & Development. If there are other authors, they declare that they have no known competing financial interests or personal relationships that could have appeared to influence the work reported in this paper.

Data availability

Data will be made available on request.

Acknowledgements

The author thanks EPSRC (grant 2602203) and Nestlé for funding this research, Professor Arnulf Materny and Dr. Patrice Donfack from Constructor University Bremen, Germany, for Raman training, the workshop staff and Dr. Riyadh Al-Asady for technical support, Adrien Six for graphic design, and the iForge makerspace at the University of Sheffield for workshop facility.

References

[1] B.L. Tardy, J.J. Richardson, L.G. Greca, J. Guo, J. Bras, O.J. Rojas, Advancing bio-based materials for sustainable solutions to food packaging, Nat. Sustain. 6 (2023) 360–367.
[2] S. Otto, M. Strenger, A. Maier-Nöth, M. Schmid, Food packaging and sustainability – consumer perception vs. correlated scientific facts: a review, J. Clean. Prod. 298 (2021) 126733.
[3] M.J. Kirwan, Handbook of Paper and Paperboard Packaging Technology, Wiley, Hoboken, NJ, 2012.
[4] L. Manzocco, S. Calligaris, M. Camerin, L. Pizzale, M.C. Nicoli, Prediction of firmness and physical stability of low-fat chocolate spreads, J. Food Eng. 126 (2014) 120–125.
[5] J.M. Aguilera, M. Michel, G. Mayor, Fat migration in chocolate: diffusion or capillary flow in a particulate solid? A hypothesis paper, J. Food Sci. 69 (2006) 167–174.
[6] E.W. Washburn, The dynamics of capillary flow, Phys. Rev. 17 (1921) 273–283.
[7] M. Dubé, M. Rost, M. Alava, Conserved dynamics and interface roughening in spontaneous imbibition: a critical overview, Europ. Phys. J. B Condens. Matter Complex Syst. 15 (2000) 691–699.
[8] Q. Meng, H. Liu, J. Wang, A critical review on fundamental mechanisms of spontaneous imbibition and the impact of boundary condition, fluid viscosity and wettability, Adv. Geo-Energy Res. 1 (2017) 1–17.
[9] M. Alava, M. Dubé, M. Rost, Imbibition in disordered media, Adv. Phys. 53 (2004) 83–175.
[10] W. Van Der Merwe, C. Maree, W. Nicol, Nature of residual liquid holdup in packed beds of spherical particles, Ind. Eng. Chem. Res. 43 (2004) 8363–8368.
[11] M. Mirzajanzadeh, V.S. Deshpande, N.A. Fleck, Water rise in a cellulose foam: By capillary or diffusional flow? J. Mech. Phys. Solids 124 (2019) 206–219.
[12] S.P. Sutera, R. Skalak, The history of Poiseuille's law, Annu. Rev. Fluid Mech. 25 (1993) 1–20.
[13] C.F. Gauss, Principia Generalia Theoriae Figurae Fluidorum in Statu Aequilibrii, in: C.F. Gauss (Ed.), Werke: Fünfter Band, Springer Berlin Heidelberg, Berlin, Heidelberg, 1877, pp. 29–77.
[14] L. Metilli, M. Francis, M. Povey, A. Lazidis, S. Marty-Terrade, J. Ray, E. Simone, Latest advances in imaging techniques for characterizing soft, multiphasic food materials, Adv. Colloid Interf. Sci. 279 (2020) 102154.
[15] L. Wu, X. Tang, T. Wu, W. Zeng, X. Zhu, B. Hu, S. Zhang, A review on current progress of Raman-based techniques in food safety: from normal Raman spectroscopy to SESORS, Food Res. Int. 169 (2023) 112944.
[16] M. Petersen, Z. Yu, X. Lu, Application of Raman spectroscopic methods in food safety: a review, Biosensors 11 (2021) 187.
[17] Y. Xu, P. Zhong, A. Jiang, X. Shen, X. Li, Z. Xu, Y. Shen, Y. Sun, H. Lei, Raman spectroscopy coupled with chemometrics for food authentication: a review, TrAC Trends Anal. Chem. 131 (2020) 116017.
[18] K. Wang, Z. Li, J. Li, H. Lin, Raman spectroscopic techniques for nondestructive analysis of agri-foods: a state-of-the-art review, Trends Food Sci. Technol. 118 (2021) 490–504.
[19] C. Qu, Y. Li, S. Du, Y. Geng, M. Su, H. Liu, Raman spectroscopy for rapid fingerprint analysis of meat quality and security: principles, progress and prospects, Food Res. Int. 161 (2022) 111805.
[20] E.M. Achata, C. Esquerre, A.A. Gowen, C.P. O'Donnell, Feasibility of near infrared and Raman hyperspectral imaging combined with multivariate analysis to assess binary mixtures of food powders, Powder Technol. 336 (2018) 555–566.
[21] S. Gupta, T. Omar, F.J. Muzzio, SEM/EDX and Raman chemical imaging of pharmaceutical tablets: a comparison of tablet surface preparation and analysis methods, Int. J. Pharm. 611 (2022) 121331.
[22] T. Firkala, A. Farkas, B. Vajna, I. Farkas, G. Marosi, Investigation of drug distribution in tablets using surface enhanced Raman chemical imaging, J. Pharm. Biomed. Anal. 76 (2013) 145–151.
[23] A. Kondo, T. Koide, T. Fukami, Evaluation of the effect of Disintegrant distribution on the dissolution behavior of pharmaceutical tablets using Raman chemical imaging, Chem. Pharm. Bull. 71 (2023) 454–458.
[24] D.L. Galata, B. Zsiros, L.A. Mészáros, B. Nagy, E. Szabó, A. Farkas, Z.K. Nagy, Raman mapping-based non-destructive dissolution prediction of sustained-release tablets, J. Pharm. Biomed. Anal. 212 (2022) 114661.
[25] C. De Bleye, P.Y. Sacré, E. Dumont, L. Netchacovitch, P.F. Chavez, G. Piel, P. Lebrun, P. Hubert, E. Ziemons, Development of a quantitative approach using surface-enhanced Raman chemical imaging: first step for the determination of an impurity in a pharmaceutical model, J. Pharm. Biomed. Anal. 90 (2014) 111–118.
[26] J. Cailletaud, C. De Bleye, E. Dumont, P.-Y. Sacré, Y. Gut, N. Leblanc, P. Letellier, Y.-M. Ginot, P. Hubert, E. Ziemons, Detection of low dose of piroxicam polymorph in pharmaceutical tablets by surface-enhanced Raman chemical imaging (SER-CI) and multivariate analysis, Int. J. Pharm. 574 (2020) 118913.
[27] R. Slipets, O. Ilchenko, C. Mazzoni, F. Tentor, L.H. Nielsen, A. Boisen, Volumetric Raman chemical imaging of drug delivery systems, J. Raman Spectrosc. 51 (2020) 1153–1159.
[28] S. Šašić, T. Prusnick, Raman chemical imaging of intact non-flat tablets in regular and high-confocal mode, Anal. Methods 12 (2020) 471–482.
[29] J. Cailletaud, C.D. Bleye, E. Dumont, P.-Y. Sacré, Y. Gut, L. Bultel, Y.-M. Ginot, P. Hubert, E. Ziemons, Towards a spray-coating method for the detection of low-dose compounds in pharmaceutical tablets using surface-enhanced Raman chemical imaging (SER-CI), Talanta 188 (2018) 584–592.
[30] M. Yamashita, H. Sasaki, K. Moriyama, Vapor phase alkyne coating of pharmaceutical excipients: discrimination enhancement of Raman chemical imaging for tablets, J. Pharm. Sci. 104 (2015) 4093–4098.

[31] N.J. Lawson, The application of laser measurement techniques to aerospace flows, Proc. Inst. Mechan. Eng. Part G: J. Aerospace Eng. 218 (2004) 33–57.
[32] A. Malarski, J. Egermann, J. Zehnder, A. Leipertz, Simultaneous application of single-shot Ramanography and particle image velocimetry, Opt. Lett. 31 (2006) 1005–1007.
[33] A. Braeuer, S.R. Engel, S. Dowy, S. Luther, J. Goldlücke, A. Leipertz, Raman mixture composition and flow velocity imaging with high repetition rates, Opt. Express 18 (2010) 24579–24587.
[34] M. Wellhausen, G. Rinke, H. Wackerbarth, Combined measurement of concentration distribution and velocity field of two components in a micromixing process, Microfluid. Nanofluid. 12 (2012) 917–926.
[35] J.B. Rosenholm, Liquid spreading on solid surfaces and penetration into porous matrices: coated and uncoated papers, Adv. Colloid Interf. Sci. 220 (2015) 8–53.
[36] F. Valoppi, P. Lassila, A. Salmi, E. Haeggström, Automated image analysis method for oil-release test of lipid-based materials, MethodsX 8 (2021) 101447.
[37] Q. Zhang, F. Mugele, P.M. Lugt, D. Van Den Ende, Characterizing the fluid–matrix affinity in an organogel from the growth dynamics of oil stains on blotting paper, Soft Matter 16 (2020) 4200–4209.
[38] J. Lange, C. Pelletier, Y. Wyser, Novel method for testing the grease resistance of pet food packaging, Packag. Technol. Sci. 15 (2002) 65–74.
[39] R.M. El-Abassy, P. Donfack, A. Materny, Visible Raman spectroscopy for the discrimination of olive oils from different vegetable oils and the detection of adulteration, J. Raman Spectrosc. 40 (2009) 1284–1289.
[40] R.M. El-Abassy, P. Donfack, A. Materny, Assessment of conventional and microwave heating induced degradation of carotenoids in olive oil by VIS Raman spectroscopy and classical methods, Food Res. Int. 43 (2010) 694–700.
[41] H.R. Charles-Williams, R. Wengeler, K. Flore, H. Feise, M.J. Hounslow, A. D. Salman, Granule nucleation and growth: competing drop spreading and infiltration processes, Powder Technol. 206 (2011) 63–71.
[42] A.L. Mundozah, J.J. Cartwright, C.C. Tridon, M.J. Hounslow, A.D. Salman, Hydrophobic/hydrophilic static powder beds: competing horizontal spreading and vertical imbibition mechanisms of a single droplet, Powder Technol. 330 (2018) 275–283.
[43] S. Mascia, M.J. Patel, S.L. Rough, P.J. Martin, D.I. Wilson, Liquid phase migration in the extrusion and squeezing of microcrystalline cellulose pastes, Eur. J. Pharm. Sci. 29 (2006) 22–34.
[44] A.E. Sáez, M.M. Yépez, C. Cabrera, E.M. Soria, Static liquid holdup in packed beds of spherical particles, AICHE J. 37 (1991) 1733–1736.
[45] S. Schwidder, K. Schnitzlein, Predicting the static liquid holdup for cylindrical packings of spheres in terms of the local structure of the packed bed, Chem. Eng. Sci. 65 (2010) 6181–6189.
[46] M. Soustelle, Thermodynamics of Surfaces and Capillary Systems, Wiley, 2016.
[47] J. Kozeny, Über kapillare Leitung des Wassers im Boden (Aufstieg, Versickerung und Anwendung auf die Bewässerung), Sitzungsber. Akad. Wiss. Wien 136 (1927) 271–309.
[48] P.C. Carman, Fluid flow through granular beds, Chem. Eng. Res. Des. 75 (1937) S32–S48.